ADVANCES IN ATMOSPHERIC SCIENCES, VOL. 32, NOVEMBER 2015, 1539–1550

Tropical Cyclone Genesis Potential Index over the Western North Pacific Simulated by CMIP5 Models

SONG Yajuan[1,2], WANG Lei[3], LEI Xiaoyan*[2], and WANG Xidong[4]

[1]*College of Physical and Environmental Oceanography, Ocean University of China, Qingdao* 266100
[2]*First Institute of Oceanography, State Oceanic Administration, Qingdao* 266061
[3]*State Key Laboratory of Tropical Oceanography, South China Sea Institute of Oceanology, Chinese Academy of Sciences, Guangzhou* 510301
[4]*Key Laboratory of Marine Environment Information Technology, State Oceanic Administration, Tianjin* 300171

(Received 13 November 2014; revised 7 April 2015; accepted 5 May 2015)

ABSTRACT

Tropical cyclone (TC) genesis over the western North Pacific (WNP) is analyzed using 23 CMIP5 (Coupled Model Intercomparison Project Phase 5) models and reanalysis datasets. The models are evaluated according to TC genesis potential index (GPI). The spatial and temporal variations of the GPI are first calculated using three atmospheric reanalysis datasets (ERA-Interim, NCEP/NCAR Reanalysis-1, and NCEP/DOE Reanalysis-2). Spatial distributions of July–October-mean TC frequency based on the GPI from ERA-interim are more consistent with observed ones derived from IBTrACS global TC data. So, the ERA-interim reanalysis dataset is used to examine the CMIP5 models in terms of reproducing GPI during the period 1982–2005. Although most models possess deficiencies in reproducing the spatial distribution of the GPI, their multi-model ensemble (MME) mean shows a reasonable climatological GPI pattern characterized by a high GPI zone along 20°N in the WNP. There was an upward trend of TC genesis frequency during 1982 to 1998, followed by a downward trend. Both MME results and reanalysis data can represent a robust increasing trend during 1982–1998, but the models cannot simulate the downward trend after 2000. Analysis based on future projection experiments shows that the GPI exhibits no significant change in the first half of the 21st century, and then starts to decrease at the end of the 21st century under the representative concentration pathway (RCP) 2.6 scenario. Under the RCP8.5 scenario, the GPI shows an increasing trend in the vicinity of 20°N, indicating more TCs could possibly be expected over the WNP under future global warming.

Key words: tropical cyclone, genesis potential index, CMIP5, western North Pacific, global warming.

Citation: Song, Y. J., L. Wang, X. Y. Lei, and X. D. Wang, 2015: Tropical cyclone genesis potential index over the western North Pacific simulated by CMIP5 models. *Adv. Atmos. Sci.*, **32**(11), 1539–1550, doi: 10.1007/s00376-015-4162-3.

1. Introduction

Tropical cyclones (TCs), known as typhoons in the western North Pacific (WNP), are one of the most disastrous weather phenomena influencing agriculture, human life, and property (Chan, 2005). TC landfall, accompanied by strong wind and heavy rainfall, can result in windstorms and flood damage. There has been growing interest in TCs because of their large socioeconomic impact. In particular, anticipated future changes in TC genesis frequency under global warming scenarios have raised concern.

With the development of computing resources and numerical models, general circulation models (GCMs) are widely employed for simulating TCs. Recent GCMs with high resolution can simulate most aspects of typhoons (Zhao et al., 2009). There are several approaches for identifying TCs in GCMs, such as examining TC statistical features in the models and analyzing the large-scale environmental variables associated with TC activities. Clearly, not all models can simulate TC characteristics realistically. Therefore, some downscaling methods have been applied to represent the spatial and temporal characteristics of TCs (Villarini and Vecchi, 2013).

A series of Coupled Model Intercomparison Projects (CMIPs), promoted by the World Climate Research Program, have provided a favorable platform to evaluate the performance of climate models in a systematic manner. Furthermore, these projects have provided a great opportunity to compare and understand the characteristics of natural phenomena under different climate conditions. Phase 5 of the CMIP (CMIP5) datasets have been employed to evaluate model abilities in simulating TCs, and to predict variation in TCs under global warming scenarios (Taylor et al., 2012). Although most of the models in CMIP5, especially for long-term integration, do not have sufficiently high resolution for

* Corresponding author: LEI Xiaoyan
Email: annylxy@fio.org.cn

reproducing specific TC activities, the large-scale environmental variables associated with TC genesis can be reproduced in the models. Therefore, we focus in this study on these large-scale environmental variables associated with TC generation, rather than on individual cyclones.

Understanding the influence of large-scale environmental factors on tropical cyclone genesis is an important problem. In the absence of a comprehensive theory, empirical methods have been used to represent the relationship between large-scale environmental factors and tropical cyclone genesis. There are a few TC indices based on large-scale environmental factors, such as the yearly genesis parameter (Gray, 1979), the modified yearly convective genesis potential index (Royer et al., 1998), and the genesis potential index (GPI) (Emanuel and Nolan, 2004). The GPI summarizes the environmental factors influencing TC genesis such as low-level vorticity, vertical wind shear, mid-level air humidity, ocean temperature, and a conditionally unstable atmosphere. Such an index represents climatological spatial and seasonal distribution of TC genesis, and the relative contribution of individual large-scale environmental factors on TC genesis may be different in different regions and on different timescales. To date, the GPI has been widely used to investigate the variation of TC genesis frequency related to climate changes (Menkes et al., 2012), as well as in the western Pacific (Zhang et al., 2010; Zhao et al., 2012; Deng et al., 2014). The GPI was developed to fit the spatial distribution and annual cycle of TC genesis at the hemispheric scale (Camargo et al., 2007), and has been employed to depict the temporal variation of TCs on the seasonal scale and in future climate (Yokoi et al., 2009). It has been shown that low-resolution models can simulate the GPI better than the genesis of TCs (Walsh et al., 2013). Considering the insufficient resolution of most CMIP5 models, evaluating the GPI is a more effective way to infer variations in TC activities.

Some studies, using coarse-resolution models, have shown there to be a decreasing trend in tropical storm frequency and a slight increase in its intensity (e.g., McDonald et al., 2005). However, another experiment with a coarse-resolution atmospheric model (T42, approximately 300 km grid spacing) indicated that the change in TC frequency was insignificant (Tsutsui, 2002). According to the Intergovernmental Panel on Climate Change Fourth Assessment Report, for models with coarse resolutions, there is no consistent evidence of large variations in either TC frequency or intensity in global warming simulation (Solomon et al., 2007). The variations in TC frequency and intensity under global warming scenarios rely on the model resolutions and physical parameterizations. Considering that CMIP5 models possess better parameterization schemes and higher horizontal resolutions than CMIP3 models, there is a need to assess CMIP5 model performances in reproducing TC activities.

In this study, because different regions have different large-scale environmental factors and air–sea interaction processes determining TC frequency and intensity (Wang et al., 2012; Wang et al., 2014), we focus on the WNP, which is the most TC-active region globally. We examine how well GCMs simulate the GPI and evaluate the future changes in large-scale environmental factors linked to TCs. This study aims to evaluate model performances in simulating the climatological GPI related to TCs in the WNP, and to investigate the changes in large-scale environmental conditions for TC genesis frequency under global warming, based on the CMIP5 models. The geographic domain of the WNP used in this study is (0°–40°N, 100°–160°E). The rest of the paper is organized as follows: Section 2 introduces the models, reanalysis datasets and the GPI used in this study. Section 3 describes the temporal and spatial variations of the GPI in CMIP5 models, in historical and future projection simulations. Finally, a discussion and conclusions are provided in section 4.

2. Data and methods

2.1. *Observation and reanalysis datasets*

To evaluate model performances, we compare the simulated results with the International Best Track Archive for Climate Stewardship (IBTrACS) global tropical cyclone data for the 24-year period of 1982–2005 (Knapp et al., 2010; www.ncdc.noaa.gov/oa/ibtracs/), which is endorsed by the World Meteorological Organization (WMO). The dataset contains the best-estimated TC positions, maximum sustained wind, and minimum central pressure. We also use the latest global reanalysis data produced by the European Centre for Medium-Range Weather Forecasts: ERA-Interim (Simmons et al., 2007); the National Center for Environmental Prediction–National Center for Atmospheric Research (NCEP–NCAR) Reanalysis-1 (Kalnay et al., 1996) and NCEP/Department of Energy (DOE) Reanalysis-2 datasets (Kanamitsu et al., 2002); and the NOAA (National Oceanic and Atmospheric Administration) Optimum Interpolation (OI) Sea Surface Temperature (SST) V2 (Reynolds et al., 2002). Atmospheric humidity, wind vectors, air temperature, and SST are derived from these datasets to construct the climatological summer mean (July–October) GPI. The monthly datasets used in this study include absolute vorticity at 850 hPa, relative humidity at 600 hPa, and vertical wind shear between 850 hPa and 200 hPa. In addition, the air temperature and humidity data at all levels in the troposphere are used to calculate the potential intensity.

2.2. *Model outputs*

The CMIP5 models are used in this study to evaluate model performances in simulating the climatological GPI related with TCs in the WNP. The 20th century simulations with 24-year periods from 23 state-of-the-art coupled models are compared with observational data. All models considered in this study are listed in Table 1, which provides information about their host centers and the resolutions of their atmospheric models. The historical simulations of the CMIP5 models are forced by observed greenhouse gas concentrations, solar radiation forcing, and aerosols during the last 150 years. The historical model outputs are available

Table 1. Climate models whose outputs are analyzed in this study.

No.	Model	Institute/country	(lon × lat)	References
1	ACCESS1.0	Commonwealth Scientific and Industrial Research Organization (CSIRO) and Bureau of Meteorology (BOM)/Australia	192 × 145	Bi et al.(2013)
2	BCC-CSM1-1	Beijing Climate Center, China Meteorological Administration/China	128 × 64	Xin et al. (2013)
3	BNU-ESM	Beijing Normal University/China	128 × 64	Ji et al.(2014)
4	CanESM2	Canadian Centre for Climate Modeling and Analysis/Canada	128 × 64	Chyleketal. (2011)
5	CCSM4	National Center for Atmospheric Research/United States	288 × 192	Gent et al. (2011)
6	FGOALS-g2	LASG, Institute of Atmospheric Physics, Chinese Academy of Sciences and CESS, Tsinghua University/China	128 × 108	Li et al. (2013)
7	FIO-ESM	The First Institute of Oceanography, State Oceanic Administration/China	128 × 64	Qiao et al. (2013)
8	GFDL-ESM2G	NOAA Geophysical Fluid Dynamics Laboratory/United States	144 × 90	Dunneetal. (2012)
9	GISS-E2-H	NASA Goddard Institute for Space Studies/United States	144 × 89	Shindelletal. (2012)
10	GISS-E2-R	NASA Goddard Institute for Space Studies/United States	144 × 89	Shindelletal. (2012)
11	HadCM3	Met Office Hadley Centre/United Kingdom	96 × 73	Pope et al. (2000)
12	HadGEM2-AO	National Institute of Meteorological Research/Korea Meteorological Administration/Korea	192 × 144	Collins et al. (2011)
13	HadGEM2-CC	Met Office Hadley Centre/United Kingdom	192 × 144	Collins et al. (2011)
14	HadGEM2-ES	Met Office Hadley Centre/United Kingdom	192 × 144	Collins et al. (2011)
15	INMCM4	Institute for Numerical Mathematics/Russia	180 × 120	Volodin et al. (2010)
16	IPSL-CM5A-LR	L'Institut Pierre-Simon Laplace/France	96 × 96	Hourdin et al. (2013)
17	IPSL-CM5A-MR	L'Institut Pierre-Simon Laplace/France	144 × 143	Hourdin et al. (2013)
18	MIROC5	Atmosphere and Ocean Research Institute (University of Tokyo), National Institute for Environmental Studies, and Japan Agency for Marine-Earth Science and Technology/ Japan	256 × 128	Watanabe et al. (2010)
19	MPI-ESM-LR	Max Planck Institute for Meteorology/Germany	192 × 96	Giorgetta et al. (2013)
20	MPI-ESM-MR	Max Planck Institute for Meteorology/Germany	192 × 96	Giorgetta et al. (2013)
21	MRI-CGCM3	Meteorological Research Institute/Japan	320 × 160	Yukimoto et al. (2011)
22	NorESM1-M	Norwegian Climate Centre/Norway	144 × 96	Bentsen et al. (2013)
23	NorESM1-ME	Norwegian Climate Centre/Norway	144 × 96	Tjiputra et al. (2013)

from 1850 to 2005. To investigate changes of the GPI under future global warming scenarios, multi-model-based future projections from the representative concentration pathway (RCP) scenarios are analyzed. Two scenario datasets, denoted as RCP8.5 and RCP2.6, which indicate the highest and lowest radiative forcing values in the year 2100 relative to pre-industrial values, are analyzed to show the variation in TC genesis under the influence of atmospheric greenhouse gases, air pollutants, land use, and land cover (Meinshausen et al., 2011; Taylor et al., 2012). The GCMs have more than one member available; only the first realization of each model is used in this study. Finally, all the model outputs with different spatial resolutions are interpolated to the same grid ($1^\circ \times 1^\circ$) using the bilinear interpolation method.

2.3. *Method*

The large-scale environmental conditions for TC generation can be evaluated by the GPI. The GPI has been widely employed to represent TC activities over the WNP, and it facilitates an easier comparison with the results from CMIP3 (Yokoi et al., 2009). The four terms of the GPI are shown below:

$$\mathrm{GPI} = |10^5\eta|^{3/2} \times (1 + 0.1V_{\mathrm{shear}})^{-2} \times \left(\frac{H}{50}\right)^3 \times \left(\frac{V_{\mathrm{pot}}}{70}\right)^3 , \tag{1}$$

where η is the absolute vorticity (s^{-1}) at 850 hPa, V_{shear} (m s^{-1}) represents the magnitude of the vertical wind shear between 850 and 200 hPa, and H (%) is the relative humidity at 600 hPa. V_{pot} (m s^{-1}), representing the maximum TC potential intensity (Emanuel, 1986, 1988, 2000) is calculated as follows:

$$V_{\mathrm{pot}}^2 = C_{\mathrm{P}}(T_{\mathrm{S}} - T_{\mathrm{o}})\frac{T_{\mathrm{S}}}{T_{\mathrm{o}}}\frac{C_{\mathrm{K}}}{C_{\mathrm{D}}}(\ln\theta_{\mathrm{e}}^* - \ln\theta_{\mathrm{e}}) , \tag{2}$$

where T_{S} is the ocean surface temperature, T_{o} is the mean outflow temperature, C_{K} is the exchange coefficient for enthalpy, and C_{D} is the drag coefficient. θ_{e}^* is the saturation equivalent potential temperature at the ocean surface, and θ_{e} is the boundary layer equivalent potential temperature. The potential intensity is indicated as the upper bound of intensity that a TC may reach under appropriate thermodynamic and dynamic conditions. The four terms representing atmospheric

vorticity, vertical wind shear, air humidity, and atmospheric potential intensity play crucial roles in TC formation. The absolute vorticity and vertical wind shear are considered as dynamic components, and the relative humidity and potential intensity are thermodynamic components.

3. Results

3.1. *Observed TC frequency and the GPI in reanalysis datasets*

We select the TCs whose genesis locations are over the WNP based on the IBTrACS dataset and calculate the spatial distributions of observed TC frequency (Fig. 1a). From the WNP to the South China Sea, the characteristics of the atmosphere and ocean provide favorable conditions for TC generation during July–October. From Fig. 1a, the TC formation frequency shows a band of high values between 10°N and 20°N, with an elliptic pattern from southeast to northwest in the WNP. There are two centers of high values: one over the sea area east of the Philippines and the other over the South China Sea. Three reanalysis datasets are used to calculate the GPI. As shown in Fig. 1b, the distribution of the GPI based on ERA-Interim has a high value patch over the WNP along 10°N. Correlation analysis shows that the GPI based on ERA-Interim corresponds to observed TC generation frequency with a correlation coefficient (CC) of 0.64. NCEP Reanalysis-1 and Reanalysis-2 seem to produce lower GPI values than ERA-Interim over the WNP, but show larger GPI offshore in Chinese seas. The GPI of NCEP Reanalysis-2 shows poor agreement with observed TC frequency, and its GPI has a lower CC with TC formation frequency. From these results, there are large inconsistencies in the distributions of GPI for different reanalysis datasets. The GPI of ERA-Interim has the highest correlation with observed TCs in terms of frequency distribution; therefore, we use ERA-Interim for the model evaluations in this study.

3.2. *GPI from CMIP5 models*

The GPI values based on the 23 CMIP5 models in the period 1982–2005 are illustrated in Fig. 2. We can use them to examine the ability of these models in reproducing the geographical pattern of large-scale variables. Most models can simulate the GPI pattern characterized by the high-value zone along 20°N, except FGOALS-g2, HadGEM2-CC, HadGEM2-ES and MIROC5. The models present a wide range of GPI values. Seven models including ACCESS1.0, CanESM2, FGOALS-g2, GISS-E2-H, HadCM3, HadGEM2-

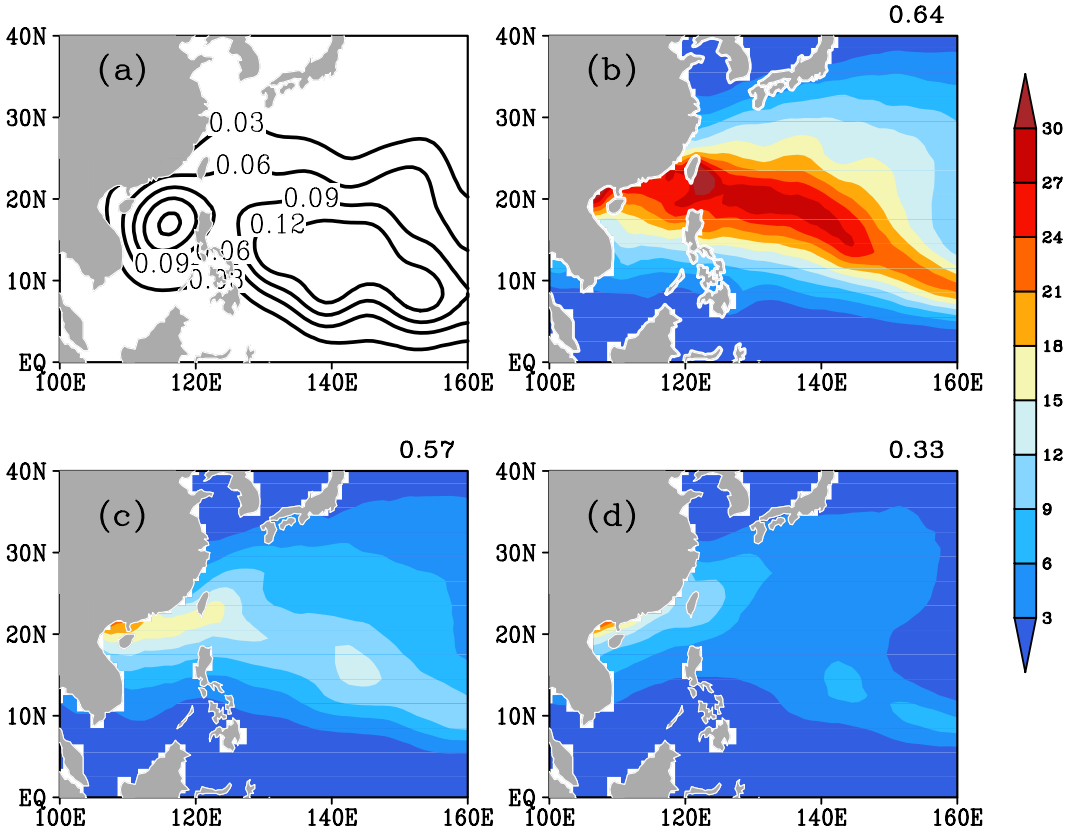

Fig. 1. (a) Spatial distributions of July–October mean frequency of observed tropical cyclone formation in the WNP. (b–d) July–October mean GPI calculated by reanalysis data. The ocean data are from OISST and the atmospheric data are from (b) ERA-Interim, (c) NCEP Reanalysis-1 and (d) NCEP Reanalysis-2.The values above each panel on the right are the correlation coefficients between observed TC frequency and the reanalysis dataset.

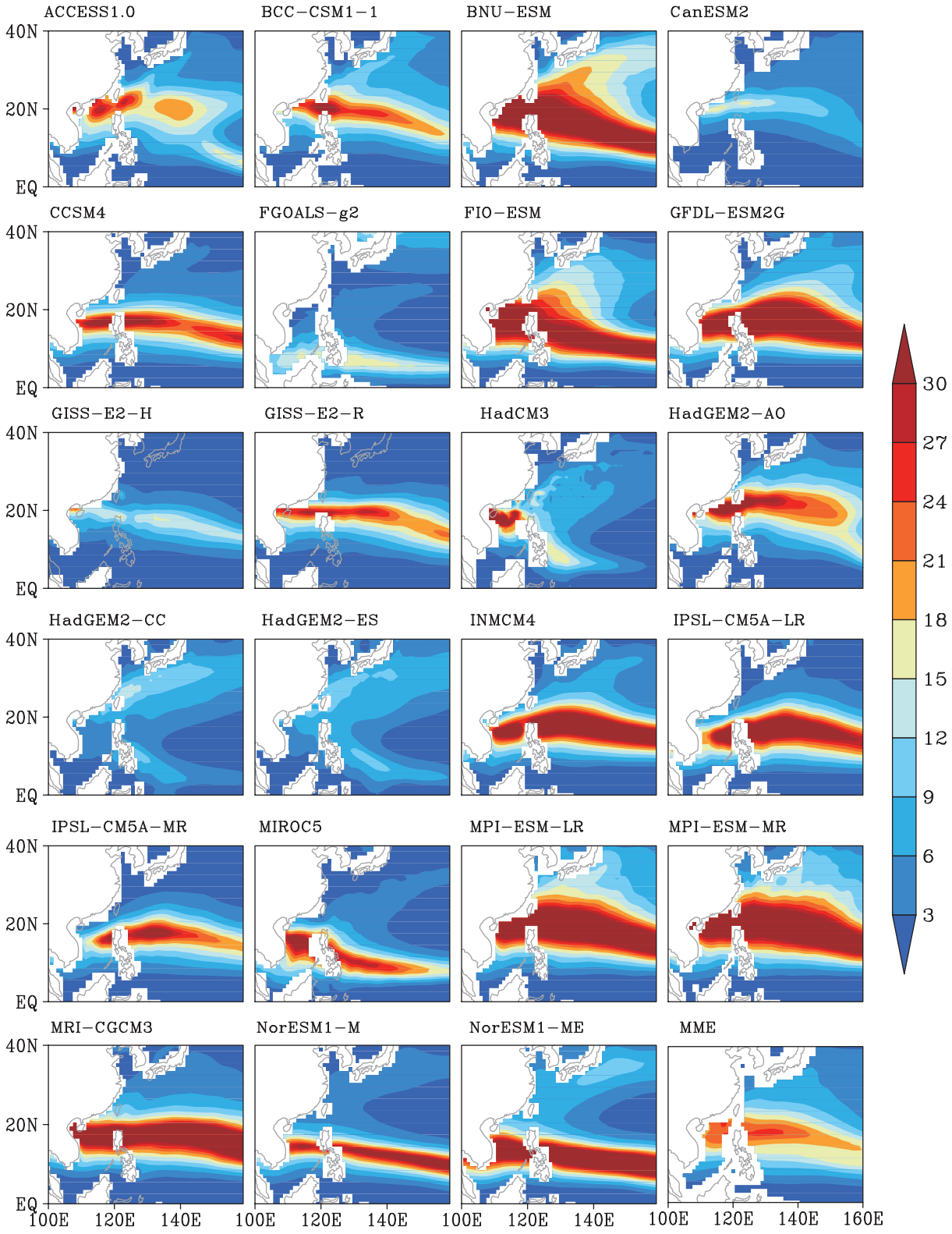

Fig. 2. July–October GPI in the WNP simulated by the CMIP5 models. MME (last panel) is the multi-model mean.

CC, and HadGEM2-ES have smaller GPI values than the other models. As shown in Fig. 2, the largest GPI values in most models are located east of the Philippines. The high-value zones in FGOALS-g2, HadCM3, HadGEM2-CC and HadGEM2-ES are closer to the equator than those in the other models. Meanwhile, four models including CanESM2, HadGEM2-AO, MPI-ESM-LR and MPI-ESM-MRI exhibit relatively small GPI values near the equator. The last panel

in Fig. 2 is the multi-model ensemble (MME) mean of the 23 model simulations. The GPI of the MME mean exhibits a zonal distribution along 20°N, which is consistent with the observed TC distributions. The conspicuous maximum of the GPI indicates that the air–sea environment provides favorable conditions for active TC frequency over the WNP along 20°N.

From Fig. 2, it is noted that the spatial distributions of the GPI simulated by the 23 CMIP5 models have large differences. The CCs and root-mean-square errors (RMSEs) between the GPI from models and the GPI from ERA-Interim–OISST reanalysis data are calculated for each of the 23 CMIP5 models (Fig. 3). The models with CCs greater than 0.5 and RMSEs less than 0.37 are selected to produce the "best model ensemble" and to carry out analysis of future global warming projections. In total, 11 climate models are selected: BCC-CSM1-1, CCSM4, FIO-ESM, GFDL-ESM2G, HadGEM2-AO, INMCM4, IPSL-CM5A-LR, IPSL-CM2A-MR, MPI-ESM-LR, MPI-ESM-MR and MRI-CGCM3. The statistical analysis shows that BCC-CSM1-1 can reproduce well the distribution of the GPI with the highest CC, but its RMSE is still larger than the MME mean. The RMSE in the MME is smaller and its CC is relatively higher than most individual models, except for BCC-CSM1-1 and MPI-ESM-MR. This indicates that the MME performs reasonably well in simulating the GPI characteristics over the WNP. Although some differences in the GPI amplitude exist between the MME mean and the reanalysis data, the general patterns of the GPI in the MME mean are in agreement with those in the reanalysis data.

The GPI differences between CMIP5 models and ERA-Interim–OISST reanalysis data are shown in Fig. 4. The GPI values in BCC-CSM1-1, CCSM4, FIO-ESM, HadGEM2-AO, IPSL-CM5A-LR and IPSL-CM5A-MR are much lower than those in the reanalysis data. Some models show negative differences in the northern part of the WNP and positive differences in the southern part, such as FIO-ESM, GFDL-ESM2G, INMCM4, IPSL-CM5A-LR, MPI-ESM-LR, MPI-ESM-MR and MRI-CGCM3.

Both the GPI and TC number exhibit significant temporal variation (Fig. 5). If we examine the long-term linear trends (as shown in Table 2), it is found that there was an upward trend of TC genesis frequency during 1982to the late 1990s, followed by a downward trend. Both ERA-Interim and NCEP Reanalysis-1showrobust increasing trends during 1982–1999, with linear trend values of 0.13 and 0.16, respectively. We also find a positive trend in the MME mean, with a trend value of 0.03. The 90% confidence interval of the MME in 1982–1999 was from −0.04 to 0.11. For the observed TC number, the 90% confidence interval is from

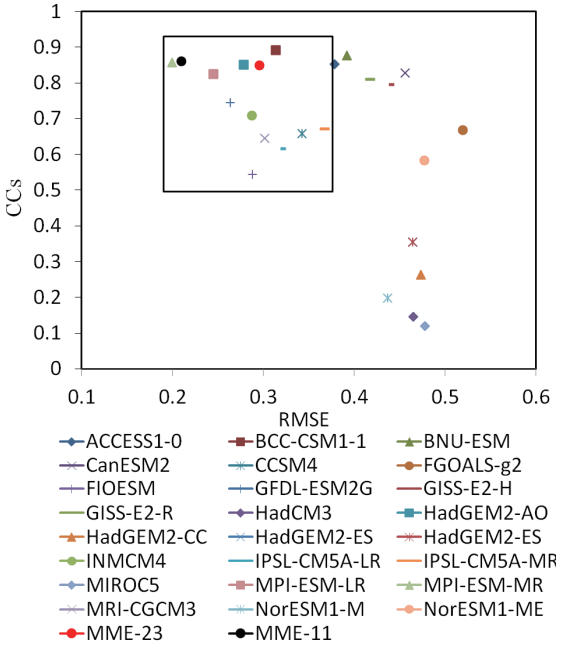

Fig. 3. Scatter plot of correlation coefficients and RMSE from CMIP5 models. The black box indicates the models used in the future projection. The red and black points represent the MME mean of correlation coefficients and RMSE based on the 23 models and 11 selected models, respectively.

−0.29 to 0.61during 1982–1999. However, the MME and ERA-Interim show upward trends in 2000–2005, which are not consistent with the trend of observed TC number. These results indicate that the variability of observed TC number and that of ERA-Interim GPI are not always consistent. The GPI is not always able to present the real TC number variations due to the limitation of the GPI and the complexity of TC activities. On the other hand, the GPI from the MME and individual models do not have to follow the observed real TC number variability, considering that the upward and downward trends of observed TC number may mainly be parts of long-term natural variability and the possible biases in individual model simulations. Due to the limitations of the GPI and the model biases, it should be noted that there are many uncertainties to assessing future change in TC number using the GPI from the CMIP5 models. For 1982–1999, 7 out of 11 models show the same upward trend as observed: CCSM4, INMCM4, IPSL-CM5A-LR, IPSL-CM5A-MR, MPI-ESM-LR, MPI-ESM-MR and MRI-CGCM3. The temporal variation of the GPI in the MME mean before 1999 is similar to observed, but it has a significant increasing trend after 1999 that is inconsistent with observations.

So, what causes the GPI biases in these models? The GPI

Table 2. Trends and 90% confidence intervals (in square brackets) of the GPI derived from different datasets and time periods.

	MME	ERA-OISST	NCEP-OISST	TC number
1982–1998	0.03[−0.04 0.1]	0.13[−0.03 0.29]	0.16[0.02 0.3]	0.15[−0.29 0.61]
1999–2005	0.04[−0.28 0.37]	0.3[−0.92 1.57]	−0.32[−0.94 0.29]	−1.14[−3.2 0.96]

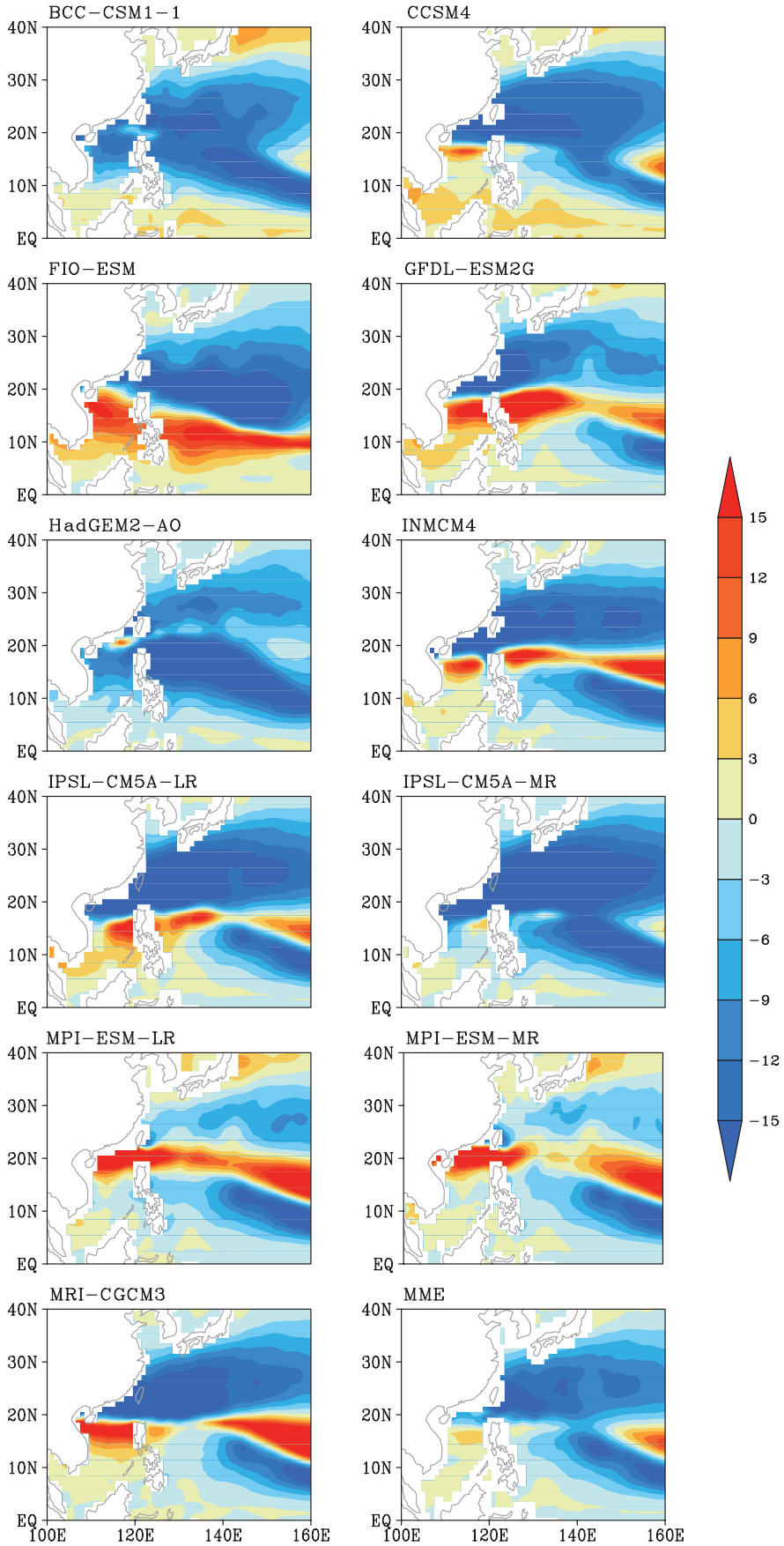

Fig. 4. GPI differences between CMIP5 models and ERA-Interim–OISST reanalysis data.

is composed of four terms; therefore, we examine those individual four terms in more detail in Fig. 6. The first term, representing atmospheric absolute vorticity, is almost the same in the MME mean and the reanalysis data. The second term, associated with vertical wind shear, is smaller in the MME than in the two reanalysis datasets in the area around Taiwan Island. Since the second term of the GPI has an inverse relationship with the vertical wind shear, it means that the simulated vertical wind shear is larger along 20°N than those of ERA-Interim and NCEP Reanalysis-1, which hinders TC generation in this region. The third term, associated with mid-level humidity, shows a robustly high value in the tropical region from the equator to 20°N in the MME. Previous studies also suggest that models usually produce a higher

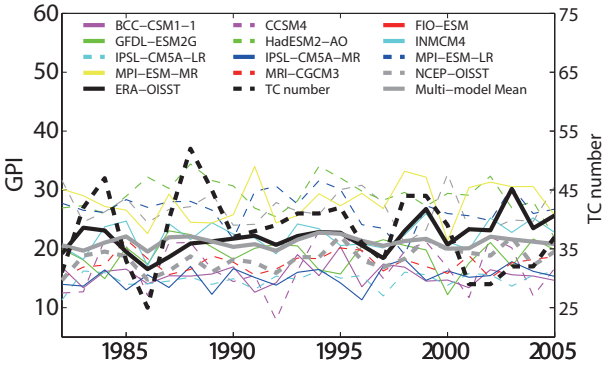

Fig. 5. GPI time series from 1982 to 2005. The dashed black curve is the TC number in the WNP (0°–30°N, 100°–160°E).

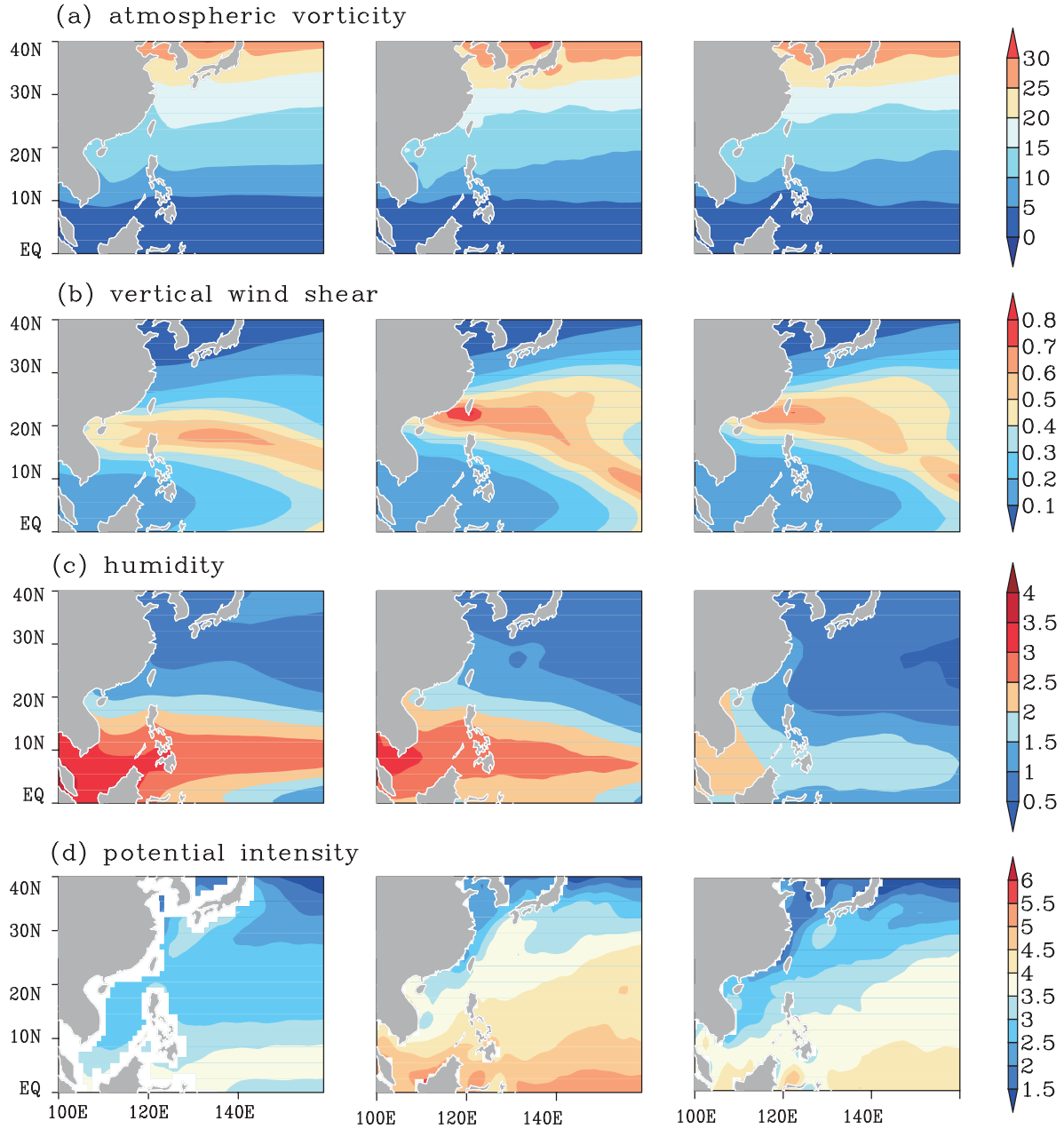

Fig. 6. Four terms of the GPI over the NWP from MME results (left), ERA-Interim–OISST data (middle) and NCEP Reanalysis-1–OISST data (right).

relative humidity than observed (Walsh et al., 2013). In this study, the humidity in the climate models is also higher than that in ERA-Interim. NCEP Reanalysis-1 shows a lower humidity compared with the MME mean and ERA-Interim. The fourth term is for potential intensity, with higher values in the low-latitude area in ERA-Interim and NCEP Reanalysis-1. The potential intensity in the MME mean is smaller than those in ERA-Interim and NCEP Reanalysis-1. In general, the second term, representing vertical wind shear, and the fourth term, associated with potential intensity, show lower values in the MME mean than the two reanalysis datasets; whereas, the atmospheric humidity in the MME mean is larger than those in the reanalysis data. By comparing the GPI from ERA-Interim and NCEP Reanalysis-1, lower GPI values in NCEP Reanalysis-1 are mainly due to lower mid-level humidity and weaker potential intensity. If we compare the GPI in the MME mean and ERA-Interim, smaller GPI values in the MME are mainly induced by weaker potential intensity.

Potential changes in GPI due to global warming are evaluated using the RCP2.6 and RCP8.5 scenarios (Fig. 7). We note that the GPI values in the two scenarios have strong interannual variations. In the RCP8.5 scenario, there is an obvious upward trend in the period 2006–2095; the trend value is 0.02 and the 90% confidence interval is from 0.01 to 0.033. This shows a high level of statistical significance. Eight out of eleven models have positive trends under RCP8.5: BCC-CSM1-1, FIO-ESM, GFDL-ESM2G, HadGEM2-AO, INMCM4, IPSL-CM5A-LR, IPSL-CM5A-MR and MRI-CGCM3. It is suggested that global warming may possibly provide favorable large-scale environmental conditions for TC formation over the WNP. On the other hand, the time series of GPI under the RCP2.6 scenario shows a negative trend of −0.002, but this is not statistically significant. Under the RCP2.6 scenario, the GPI exhibits no significant trend before 2060 in the 21st century, and only decreases at the end of the 21st century.

A point of interest is the spatial characteristics of the GPI under global warming. We use 11 models including BCC-CSM1-1, CCSM4, FIO-ESM, GFDL-ESM2G, HadGEM2-AO, INMCM4, IPSL-CM5A-LR, IPSL-CM2A-MR, MPI-ESM-LR, MPI-ESM-MR and MRI-CGCM3 under the highest scenario RCP8.5to demonstrate the change. As shown in Fig. 8, the differences in GPI between RCP8.5 (2076–2100) and historical simulations (1982–2005) in the WNP have two positive value patches along 15°N and 25°N. In the South China Sea, the GPI has a downward trend in the north (north of 17°N) and an upward trend in the south (between 10°N and 17°N). The changes in the GPI result in an out-of-phase relationship between TCs formed in the north and south. In the WNP, the GPI differences show a positive anomaly with two centers of large value in the region east of Taiwan from 20°N to 30°N and east of the Philippines from 10°N to 20°N, where typhoons frequently occur. The result suggests that the WNP, especially from 10°N to 30°N, may be expected to have more cyclone genesis under the global warming scenarios. The correlation coefficients between each model's

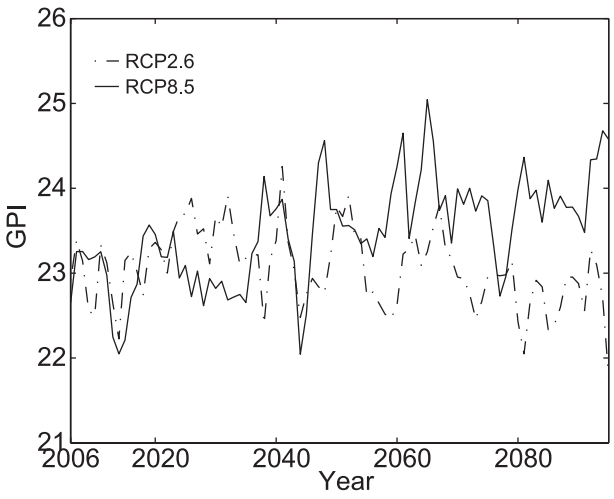

Fig. 7. Time series of MMEGPI under the RCP scenarios in the domain (5°–30°N, 110°–160°E).

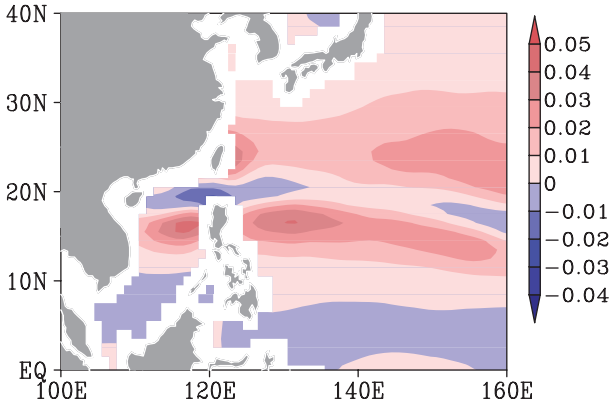

Fig. 8. Differences in MMEGPI between RCP8.5 (2076–2100) and historical simulations (1982–2005).

difference and the MME results are calculated. Eight of eleven models have CCs greater than 0.5, and the CCs of five models are greater than 0.8. Correlation analysis shows that most models project the same pattern as the MME under RCP8.5. The differences in the four terms between RCP8.5 and historical simulations are shown in Fig. 9. For absolute vorticity, there is a positive anomaly north of 20°N and a negative anomaly to the south (Fig. 9a). The distributional characteristics of the second term, related to vertical wind shear, show similar patterns, with a positive anomaly lying further south, extending from the South China Sea to the WNP. Both the absolute vorticity and vertical wind shear are out of phase in the zonal direction in the WNP. This means that TCs would increase in the northern part of the WNP and decrease in the southern part of the WNP. In addition, both relative humidity and potential intensity differences produce positive values over almost the whole of the WNP. The differences in the GPI between RCP8.5 and historical simulations have larger correlation coefficients with the differences of the third term, indicating that the change in the GPI under RCP8.5 is mainly

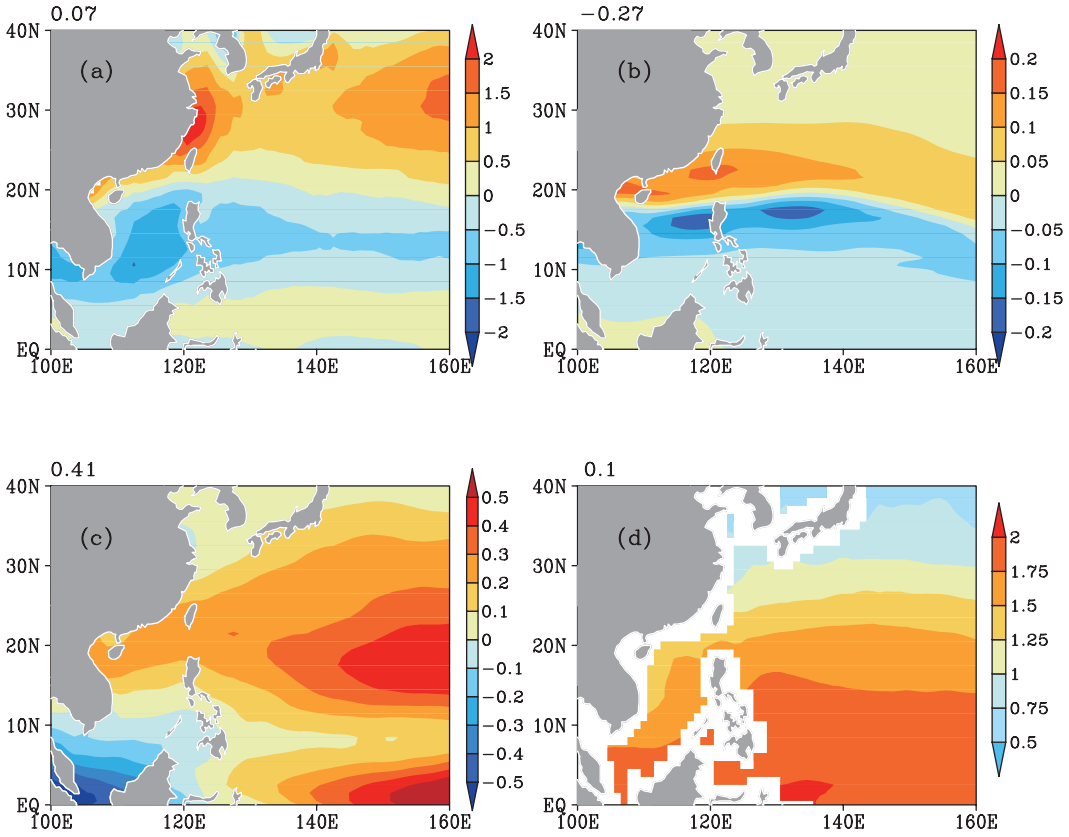

Fig. 9. Differences in the four terms in the GPI between RCP8.5 (2076–2100) and historical simulations (1982–2005): (a) absolute vorticity; (b) vertical wind shear; (c) relative humidity; and (d) potential intensity. The value above each panel on the left is the correlation coefficient between the difference in the GPI (as shown in Fig. 8) and the differences of each term.

caused by changes in relative humidity.

4. Discussion and conclusions

This study has assessed the GPI over the WNP in CMIP5 models. Three reanalysis datasets including ERA-Interim, NCEP Reanalysis 1, and NCEP/DOE Reanalysis 2 were first evaluated using the IBTrACS best track data. Based on the climatology of the 20th century, most of the 23 models still show deficiencies in terms of geographical patterns of the GPI in the WNP and produce a wide range of index values over time. Their MME mean reasonably represents the GPI distributions characterized by a large-value region from the South China Sea to the western Pacific, which are consistent with those in the observation and reanalysis products. Eleven out of 23 models with higher CCs and lower RMSEs were used to present the GPI variation over time. The GPI exhibits an increasing trend in both reanalysis data and the MME mean during the period 1982–1999. Analysis based on future projection experiments showed that the GPI under the RCP2.6 scenario has no significant change in the first half of the 21st century and then decreases at the end of the 21st century, while the GPI under RCP8.5 exhibits an increasing trend. The GPI differences between RCP8.5 and historical results showed that there are bands of positive values along 15°N and 25°N, suggesting that more TCs could possibly be expected over the WNP under future global warming, particularly over this two-band region. By examining the four terms in the GPI, it was found that the changes in the GPI under RCP8.5 are mainly caused by changes in relative humidity.

Many models, owing to their low resolutions, produce much weaker and larger TCs (Camargo et al., 2005). Although the model resolutions in CMIP5 are higher compared with the GCMs in CMIP3, they are still insufficient for reproducing TC structures and spatiotemporal distributions. Considering the insufficient resolution of most CMIP5 models, evaluating the GPI is a more effective way to infer variations in TC activities. This study has provided an evaluation of CMIP5 model performances in simulating the GPI in the WNP and an investigation of the changes in large-scale environmental conditions associated with TC genesis under global warming. However, it should be noted that there are many uncertainties in future TC projection from the GPI. The GPI is not always able to present the actual TC variations due to the limitation of the GPI and the complexity of TC activities. In this study, information on the GPI under RCP2.6 and RCP8.5 has been presented, which provides only some clues and possible information on future TC projection. Although TC frequency cannot be determined by the GPI in an

absolutely accurate way, it could still provide some helpful information and clues to understanding the possible changes in TC activities.

Acknowledgements. This study was supported by the National Basic Research Program of China (973 Program) (Grant No. 2013CB430304), the Scientific Research Foundation of the First Institute of Oceanography, the State Oceanic Administration (Grant No.GY0213G19), and the National Natural Science Foundation of China (Grant Nos.41205026 and41206026). WL was also supported by the Strategic Priority Research Program of the Chinese Academy of Sciences (Grant No.XDA11010104) and the Knowledge Innovation Program of the Chinese Academy of Sciences (Grant No. SQ201208). The authors wish to thank the ESG-PCMDI for providing the CMIP5 model outputs.

REFERENCES

Bentsen, M., and Coauthors, 2013: The Norwegian Earth System Model, NorESM1-M-Part 1: Description and basic evaluation of the physical climate. *Geoscientific Model Development*, **6**, 687–720.

Bi, D. H., and Coauthors, 2013: The ACCESS coupled model: Description, control climate and evaluation. *Australian Meteorological and Oceanographic Journal*, **63**, 41–64.

Camargo, S. J., A. G. Barnston, and S. E. Zebiak, 2005: A statistical assessment of tropical cyclone activity in atmospheric general circulation models. *Tellus A*, **57**, 589–604.

Camargo, S. J., K. A. Emanuel, and A. H. Sobel, 2007: Use of a genesis potential index to diagnose ENSO effects on tropical cyclone genesis. *J. Climate*, **20**, 4819–4834.

Chan, J. C. L., 2005: Interannual and interdecadal variations of tropical cyclone activity over the western North Pacific. *Meteor. Atmos. Phys.*, **89**, 143–152.

Chylek, P., J. Li, M. K. Dubey, M. Wang, and G. Lesins, 2011: Observed and model simulated 20th century Arctic temperature variability: Canadian Earth System Model CanESM2. *Atmos. Chem. Phys.*, **11**, 22893–22907.

Collins, W. J., and Coauthors, 2011: Development and evaluation of an Earth-System model-HadGEM2. *Geoscientific Model Development*, **4**, 1051–1075.

Deng, S. R., L. G. Wu, R. F. Wang, and C. Wang, 2014: Analysis of tropical cyclone genesis potential index with multiple reanalysis data. *Chinese J. Meteor. Sci.*, **34**, 243–251. (in Chinese)

Dunne, J. P., and Coauthors, 2012: GFDL's ESM2 global coupled climate-carbon earth system models. Part I: Physical formulation and baseline simulation characteristics. *J. Climate*, **25**, 6646–6665.

Emanuel, K. A., 1986: An air-sea interaction theory for tropical cyclones. Part I: Steady-state maintenance. *J. Atmos. Sci.*, **43**, 585–605.

Emanuel, K. A., 1988: The maximum intensity of hurricanes. *J. Atmos. Sci.*, **45**, 1143–1155.

Emanuel, K, 2000: A statistical analysis of tropical cyclone intensity. *Mon. Wea. Rev.*, **128**, 1139–1152.

Emanuel, K. A., and D. S. Nolan, 2004: Tropical cyclone activity and the global climate system. *Preprints*, 26*th Conf. on Hurricanes and Tropical Meteorology*, Miami, FL, Amer. Meteor.Soc., 240–241.

Gent, P. R., and Coauthors, 2011: The community climate system model version 4. *J. Climate*, **24**, 4973–4991.

Giorgetta, M. A., and Coauthors, 2013: Climate and carbon cycle changes from 1850 to 2100 in MPI-ESM simulations for the Coupled Model Intercomparison Project phase 5. *Journal of Advances in Modeling Earth Systems*, **5**, 572–597.

Gray, W. M., 1979: Hurricanes: Their formation, structure and likely role in the tropical circulation. *Meteorology over the Tropical Oceans*, D. B. Shaw, Ed., Royal Meteor. Soc., James Glaisher House, Grenville Place, Bracknell, Berkshire, 155–218.

Hourdin, F., and Coauthors, 2013: LMDZ5B: The atmospheric component of the IPSL climate model with revisited parameterizations for clouds and convection. *Climate Dyn.*, **40**, 2193–2222.

Ji, D., and Coauthors, 2014: Description and basic evaluation of Beijing Normal University Earth System Model (BNU-ESM) version 1. *Geoscientific Model Development*, **7**, 2039–2064.

Kalnay, E., and Coauthors, 1996: The NCEP/NCAR 40-year reanalysis project. *Bull. Amer. Meteor. Soc.*, **77**, 437–470.

Kanamitsu, M, W. Ebisuzaki, J. Woollen, S.-K. Yang, J. J. Hnilo, M. Fiorino, and G. L. Potter, 2002: NCEP-DOE AMIP-II reanalysis (R-2). *Bull. Amer. Meteor. Soc.*, **83**, 1631–1643.

Knapp, K. R., M. C. Kruk, D. H. Levinson, H. J. Diamond, and C. J. Neumann, 2010: The International best Track archive for climate stewardship (IBTrACS). *Bull. Amer. Meteor. Soc.*, **91**, 363–376.

Li, L. J., and Coauthors, 2013: The flexible global ocean-atmosphere-land system model, Grid-point Version 2: FGOALS-g2. *Adv. Atmos. Sci.*, **30**, 543–560, doi: 10.1007/s00376-012-2140-6.

McDonald, R. E., D. G. Bleaken, D. R. Cresswell, V. D. Pope, and C. A. Senior, 2005: Tropical storms: Representation and diagnosis in climate models and the impacts of climate change. *Climate Dyn.*, **25**, 19–36.

Meinshausen, M., and Coauthors, 2011: The RCP greenhouse gas concentrations and their extensions from 1765 to 2300. *Climatic Change*, **109**, 213–241.

Menkes, C. E., M. Lengaigne, P. Marchesiello, N. C. Jourdain, E. M. Vincent, J. Lefèvre, F. Chauvin, and J.-F. Royer, 2012: Comparison of tropical cyclogenesis indices on seasonal to interannual timescales. *Climate Dyn.*, **38**, 301–321.

Pope, V. D., M. L. Gallani, P. R. Rowntree, and R. A. Stratton, 2000: The impact of new physical parametrizations in the Hadley Centre climate model: HadAM3. *Climate Dyn.*, **16**, 123–146.

Qiao, F., Z. Song, Y. Bao, Y. Song, Q. Shu, C. Huang, and W. Zhao, 2013: Development and evaluation of an earth system model climate with surface gravity waves. *J. Geophys. Res. Oceans*, **118**, 4514–4524.

Reynolds, R. W., N. A. Rayner, T. M. Smith, D. C. Stokes, and W. Q. Wang, 2002: An improved in situ and satellite SST analysis for climate. *J. Climate*, **15**, 1609–1625.

Royer, J.-F., F. Chauvin, B. Timbal, P. Araspin, and D. Grimal, 1998: A GCM study of the impact of greenhouse gas increase on the frequency of occurrence of tropical cyclones. *Climatic Change*, **38**, 307–343.

Shindell, D. T., and Coauthors, 2012: Interactive ozone and methane chemistry in GISS-E2 historical and future climate simulations. *Atmos. Chem. Phys.*, **13**, 2653–2689.

Simmons, A. J., S. M. Uppala, D. P. Dee, and S. Kobayashi, 2007: ERA-Interim: New ECMWF reanalysis products from 1989

onwards. *ECMWF Newsletter*, **110**, 25–35.

Solomon, S., D. Qin, M. Manning, Z. Chen, M. Marquis, K. B. Averyt, M. Tignor, and H. L. Miller, 2007: Climate Change 2007: The Physical Science Basis. *Contribution of Working Group I to the Fourth Assessment Report of the Intergovernmental Panel on Climate Change*, Cambridge University Press, Cambridge, United Kingdom and New York, NY, USA, 996 pp.

Taylor, K. E., R. J. Stouffer, and G. A. Meehl, 2012: An overview of CMIP5 and the experiment design. *Bull. Amer. Meteor. Soc.*, **93**, 485–498.

Tjiputra, J. F., C. Roelandt, M. Bentsen, D. M. Lawrence, T. Lorentzen, J. Schwinger, Ø. Seland, and C. Heinze, 2013: Evaluation of the carbon cycle components in the Norwegian Earth System Model (NorESM). *Geoscientific Model Development*, **6**, 301–325.

Tsutsui, J., 2002: Implications of anthropogenic climate change for tropical cyclone activity: A case study with the NCAR CCM2. *J. Meteor. Soc. Japan*, **80**, 45–65.

Villarini, G., and G. A. Vecchi, 2013: Projected increases in North Atlantic tropical cyclone intensity from CMIP5 models. *J. Climate*, **26**, 3231–3240.

Volodin, E. M., N. A. Diansky, and A. V. Gusev, 2010: Simulating present-day climate with the INMCM4.0 coupled model of the atmospheric and oceanic general circulations. *Izvestiya. Atmospheric and Oceanic Physics*, **46**, 414–431.

Walsh, K., S. Lavender, E. Scoccimarro, and H. Murakami, 2013: Resolution dependence of tropical cyclone formation in CMIP3 and finer resolution models. *Climate Dyn.*, **40**, 585–599.

Wang, X., W. Zhou, C. Y. Li, and D. X. Wang, 2012: Effects of the East Asian summer monsoon on tropical cyclone genesis over the South China Sea on an interdecadal timescales. *Adv. Atmos. Sci.*, **29**, 249–262, doi: 10.1007/s00376-011-1080-x.

Wang, X., W. Zhou, C. Y. Li, and D. X. Wang, 2014: Comparison of the impact of two types of El Niño on tropical cyclone genesis over the South China Sea. *Int. J. Climatol.*, **34**, 2651–2660.

Watanabe, M., and Coauthors, 2010: Improved climate simulation by MIROC5: Mean states, variability, and climate sensitivity. *J. Climate*, **23**, 6312–6335.

Xin, X. G., T. W. Wu, J. L. Li, Z. Z. Wang, W. P. Li, and F. H. Wu, 2013: How well does BCC_CSM1.1 reproduce the 20th century climate change over China?. *Atmos. Oceanic Sci. Lett.*, **6**, 21–26.

Yokoi, S., Y. N. Takayabu, and J. C. L. Chan, 2009: Tropical cyclone genesis frequency over the western North Pacific simulated in medium-resolution coupled general circulation models. *Climate Dyn.*, **33**, 665–683.

Yukimoto, S., and Coauthors, 2011: Meteorological Research Institute-Earth System Model Version 1 (MRI-ESM1)-Model Description. Technical Reports of the Meteorological Research Institute No.64, Meteorological Research Institute, Tsukuba, Japan, 83 pp.

Zhang Y., H. J. Wang, J. Q. Sun, and H. Drange, 2010: Changes in the tropical cyclone genesis potential index over the western North Pacific in the SRES A2 scenario. *Adv. Atmos. Sci.*, **27**, 1246–1258, doi: 10.1007/s00376-010-9096-1.

Zhao, J. P., L. G. Wu, and H. K. Zhao, 2012: Improvement of tropical cyclone genesis potential index in the western North Pacific Basin. *Journal of the Meteorological Sciences*, **32**, 591–599. (in Chinese)

Zhao, M., I. M. Held, S.-J.Lin, and G. A. Vecchi, 2009: Simulations of global hurricane climatology, interannual variability, and response to global warming using a 50-km resolution GCM. *J. Climate*, **22**, 6653–6678.